

# Mode I Fracture Toughness of Nanorubber Modified Epoxy under Wide loading Rate

Ying-Gang Miao<sup>1,2</sup>, Hong-Yuan Liu<sup>2\*</sup>, Yu-Long Li<sup>1\*</sup>, Hsiu Hsien Wu<sup>2</sup>, and Yiu-Wing Mai<sup>2</sup>

<sup>1</sup> School of Aeronautics, Northwestern Polytechnical University, Xi'an, Shaanxi Province, 710072, P.R.China

<sup>2</sup> Center for Advanced Materials Technology (CAMT), School of Aeronautics, Mechanical & Mechatronic Engineering J07, The University of Sydney, Sydney, NSW 2006, Australia

Corresponding Authors: [hong-yuan.liu@sydney.edu.au](mailto:hong-yuan.liu@sydney.edu.au) (H-Y Liu);  
[liyulong@nwpu.edu.cn](mailto:liyulong@nwpu.edu.cn) (Y-L Li)

## Abstract

Dynamic mode I fracture toughness of nano-rubber modified epoxy were investigated using the split Hopkinson tension bar (SHTB) facility, with loading rates up to  $3 \times 10^4$  MPa $\cdot\sqrt{m/s}$ . The quasi-static toughness of those nanocomposites were also measured with an Instron machine at two loading rates of  $\sim 0.04$  MPa $\cdot\sqrt{m/s}$  and  $5$  MPa $\cdot\sqrt{m/s}$ , respectively. The materials tested are: neat epoxy; and 2, 6 and 10 wt.% nano-rubber particles, respectively, in epoxy. Special specimens with a single-edge crack in the finite width direction were designed for mode I toughness testing with the SHTB. In addition, pulse shaping technique was used to optimize the loading stress wave for accurate measurements with the SHTB. The results indicated that the presence of nano-rubber could improve the fracture toughness of the bulk composites in the range of loading rates studied. However, high loading rates might have degraded the cavitation capability of the nano-rubber and hence decreased the toughness of the rubber-modified epoxies compared to low loading rates.

**Keywords** Nano-rubber modified epoxy, fracture toughness, high strain rate, Hopkinson bar

## 1. Introduction

Epoxies have gained growing attention from industries for its specific properties, such as high modulus and strength. Epoxy products have also been widely used as structural materials, e.g., window of vehicles and helmet to resist impact and explosion. However, the low toughness of epoxy is always the disadvantage in its applications. The advent of nanoparticles has offered one excellent candidate for toughening epoxy to satisfy specific engineering requirements. To add soft or rigid nano-fillers to epoxy can significantly enhance the toughness of epoxy with no serious loss in strength and elastic modulus [1-2]. Owing to the expanded applications of epoxy products, their dynamic responses have drawn increasing attention from both industry and scientific communities, though some polymers have been investigated extensively under quasi-static loading. Sahraoui [3] studied the fracture behaviors of a modified epoxy resin by three different testing machines with loading rates in the range from  $5 \times 10^3$  to  $10^4$  MPa $\cdot\sqrt{m/s}$ . Evora [4] measured dynamic fracture

toughness of polyester/TiO<sub>2</sub> nanocomposites with three-point bend specimens, which were higher than their quasi-static fracture toughness. However, there is little known on the dynamic fracture behaviors of epoxies filled with soft nano-rubber particles at high loading rates. But, such results are necessary to understand their performance and reliability as structural materials under those extreme conditions. In this study, ~100 nm diameter nano-rubber particles were used to process epoxy composites and prepare single-edge notched specimens for dynamic toughness measurements with a split Hopkinson tensile bar (SHTB) at a maximum loading rate of  $3 \times 10^4$  MPa·√m/s. Toughness tests at lower quasi-static rates were also conducted on an Instron machine and the results were analyzed.

## 2. Materials and specimen

The resin selected was standard diglycidyl ether of bisphenol A (DGEBA) with an epoxide equivalent weight (EEW) of 185 g/mol and Araldite-F was supplied by Sigma-Aldrich in Australia. Spherical rubber particles ~100 nm with excellent dispersion were supplied with 25 wt.% (weight percent) concentration in bisphenol A resin by Kaneka Corporation, Japan. The curing agent was a cycloaliphatic secondary amine, Piperidine, obtained from Sigma-Aldrich.

Material formulations were prepared by mixing plain DGEBA resin with required amounts of nano-rubber master batch. Three weight fractions of nano-rubber particles were made, 2 wt.%, 6 wt.% and 10 wt.% nano-rubber particles in epoxy (denoted by R2, R6 and R10 hereafter), respectively. Samples with neat epoxy were also made to study the effect of nano-rubber. After adding the curing agent to the mixture, it was poured into two pre-heated moulds for curing at 120°C for 16 h. One mould was fabricated for Compact Tension (CT) specimens following ASTM D5045-99 [5]; the other was for making bulk materials, which were cut into beams  $4.5 \times 14 \times 65$  mm<sup>3</sup> for dynamic fracture tests. Figure 1 shows the TEM microstructures of R10, which indicates clearly nanoparticles dispersed uniformly in the epoxy matrix.

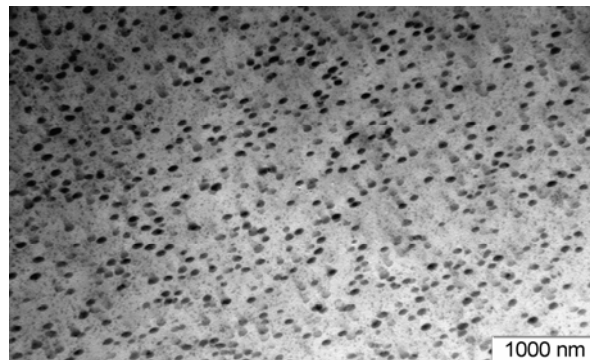


Figure 1. Nano-rubber dispersion of R10

All samples were first heated for 2 h at 80°C to remove any residual stress owing to surface polishing. A natural crack was then obtained by tapping a fresh razor blade at a specimen notch tip. The length  $a$  of the CT specimens was between  $0.45W$  and  $0.55W$  [5].



Figure 2. Quasi-static testing of CT specimen with the loading fixture

### 3: Experimental Work

#### 3.1 Quasi-static fracture toughness tests with CT samples

Quasi-static tests were conducted on CT specimens in a screw-driven Instron 5567 machine with full control of loading rates in the range of 1 to 100 mm/min and full records of load and displacement (see Figure 2).

#### 3.2 Dynamic fracture experiments

Dynamic fracture toughness tests were conducted on the SHTB facility to obtain the tensile stress-strain curves at high strain rates from  $10^2$  to  $10^3$  s<sup>-1</sup> [6, 7]. SHTB consists basically of a striker tube, an incident bar and a transmitted bar (see Figure 3). The specimen was cemented between the incident and transmitted bars.

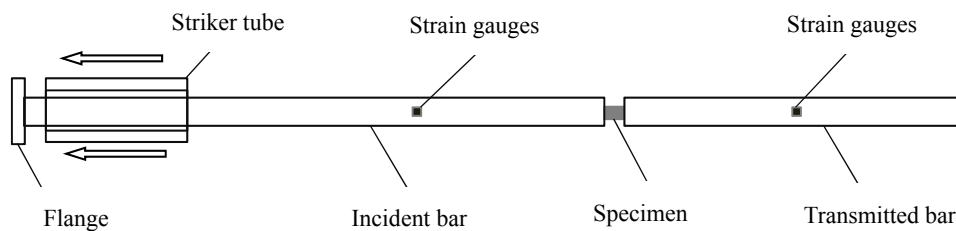


Figure 3. Schematic drawing of the SHTB test

While testing, the striker tube was projected towards the flange by a gas gun. Upon impacting, an incident wave  $\epsilon_i(t)$  was generated, and reflected at the flange free end, presenting tensile stress wave, and then propagated backwards to the interface between the incident bar and the specimen. At this interface, part of the incident wave,  $\epsilon_r(t)$  was reflected back into the incident bar. The rest went through the specimen and, finally developed the transmitted wave,  $\epsilon_t(t)$  in the transmitted bar. The incident, reflected and transmitted waves were recorded by the strain gauges and the dynamic strain recording machine.

From one-dimensional wave theory, the stress at the bar end is given by:

$$\sigma_I(t) = E(\varepsilon_i(t) + \varepsilon_r(t)) \quad (1)$$

$$\sigma_T(t) = E\varepsilon_t(t) \quad (2)$$

where  $E$  is Young's modulus of incident and transmitted bars;  $\varepsilon_r(t)$  and  $\varepsilon_t(t)$  are reflected and transmitted waves, respectively. Aluminum bars 15 mm diameter were used. Impact velocities of the striker tube were applied by controlling the pressure of the gas gun to achieve desired loading rates. Specimens were designed to suit the Hopkinson bars and essentially single-edge notched tension (SENT) geometry (see Figure 4).

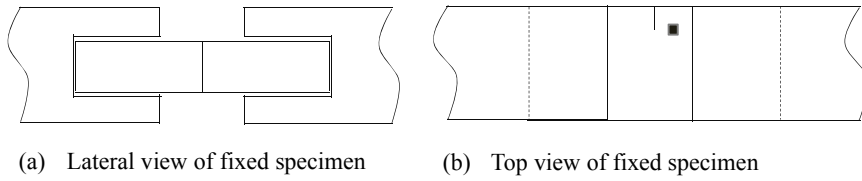


Figure 4 Fixture of dynamic toughness specimen and arrangements of strain gauge and crack

The specimen, with the size of  $4.5\text{mm} \times 14\text{mm} \times 65\text{mm}$ , was cemented and embedded 20 mm into the bars. The strain gauge glued near the crack-tip was used to ascertain the crack initiation time [8]. The pulse shaping technique was employed to trim and optimize the incident stress, and to achieve stress equilibrium in the specimen in a short time [9]. At least 3 repeated tests were conducted for each material.

## 4. Results and Discussion

### 4.1 Calculation of fracture toughness

For the CT tests, the fracture toughness is calculated by [5]

$$K_{IC} = \frac{P}{B\sqrt{W}} f(a/W) \quad (3)$$

where  $P$  is fracture initiation load, and

$$f\left(\frac{a}{W}\right) = f(\alpha) = \frac{2+\alpha}{(1-\alpha)^{3/2}} (0.886 + 4.64\alpha - 13.32\alpha^2 + 14.73\alpha^3 - 5.6\alpha^4) \quad (4)$$

For the SENT specimen under dynamic loading, the fracture toughness is obtained from [10]

$$K_{IC} = \sigma\sqrt{\pi a} \cdot F_I(\alpha), \alpha = \frac{a}{W} \quad (5)$$

where  $\sigma$  is fracture stress on the specimen width, and

$$F_I(\alpha) = 1.12 - 0.231\alpha + 10.55\alpha^2 - 21.72\alpha^3 + 30.39\alpha^4 \quad (6)$$

The fracture stress  $\sigma$  is calculated from the transmitted stress  $\sigma_T$ :

$$\sigma(t) = \frac{A_{Bar}}{A_{Specimen}} \sigma_T(t) \quad (7)$$

In all the tests, the loading rate is defined by:

$$\dot{K}_I = \frac{K_{IC}}{t_c} \quad (8)$$

where  $K_{IC}$  is critical stress intensity factor and  $t_c$  is time interval from the start of loading to when the crack starts to propagate. A typical load-time curve recorded by the Instron machine for a CT specimen is shown in figure 5.

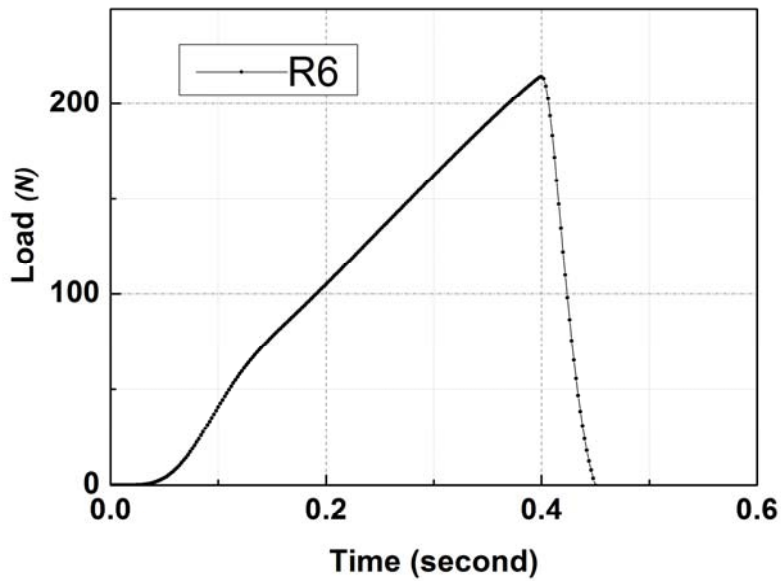


Figure 5 Load-time curve of a R6 CT specimen under a crosshead rate of 100 mm/min

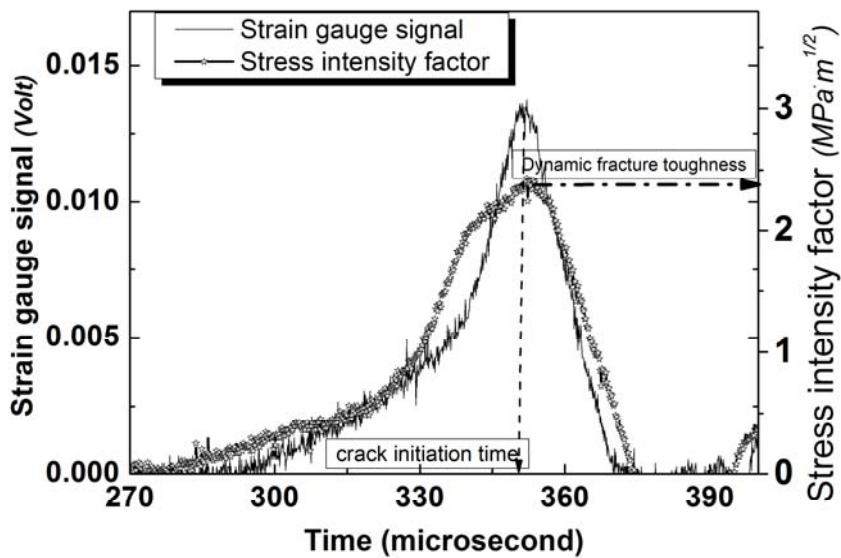


Figure 6 Toughness-time and strain signal-time curves of R6 from SHTB test

For the dynamic toughness tests, it is essential to ascertain the critical time at crack initiation. The strain measured from the strain gauge would drop dramatically when the crack was about to propagate because the strains accumulated around the crack-tip would be released once the crack moved away. Figure 6 shows the strain signal-time curve from which the stress intensity factor-time curve can be determined.

The quasi-static loading rates were  $0.04 \text{ MPa}\cdot\sqrt{\text{m}}/\text{s}$  for the crosshead rate of  $1 \text{ mm}/\text{min}$  and  $5 \text{ MPa}\cdot\sqrt{\text{m}}/\text{s}$  for  $100 \text{ mm}/\text{min}$ , respectively. The SHTB tests gave a much higher loading rate at  $\sim 3 \times 10^4 \text{ MPa}\cdot\sqrt{\text{m}}/\text{s}$ . The results of all tested materials are shown in Figure 7.

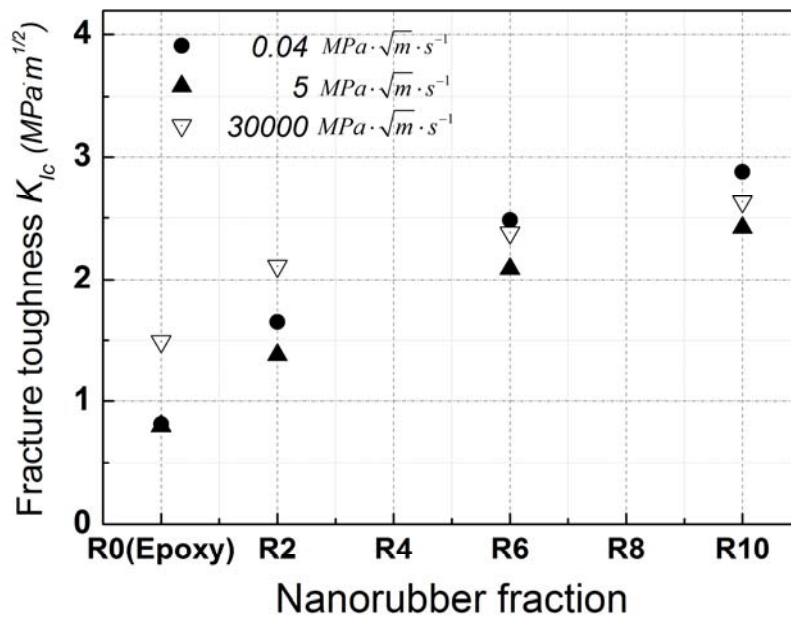


Figure 7 Effect of loading rate and nano-rubber weight fraction on fracture toughness

#### 4.2 Nano-rubber fraction and loading rate effects

Figure 7 shows clearly the improving toughening effect with increasing nano-rubber fraction. This trend is true for all three loading rates implying nano-rubber particles can improve the toughness of epoxy even at a high loading rate. However, compared to the lower loading rates, 5 and  $0.4 \text{ MPa}\cdot\sqrt{\text{m}}/\text{s}$ , the toughness increased by the rubber content under high loading rate,  $3 \times 10^4 \text{ MPa}\cdot\sqrt{\text{m}}/\text{s}$ , is less significant. For example, under quasi-static loading,  $0.04 \text{ MPa}\cdot\sqrt{\text{m}}/\text{s}$ , the toughness of R6 is more than 3.0 times the toughness of epoxy. But under high loading rate,  $3 \times 10^4 \text{ MPa}\cdot\sqrt{\text{m}}/\text{s}$ , the toughness of R6 is only  $\sim 1.8$  times the toughness of epoxy. It is possible that rubber particle cavitation is reduced due to the increased cavitation strength of the nanorubber under high loading rate. Future study will be conducted to clarify the rubber particle toughening mechanisms under different loading rates.

The results in Figure 7 show the crack growth responding to different loading rates. For neat epoxy, the toughness  $K_{ICm}$  is  $\sim 1.8$  times larger at the dynamic loading rate of  $3 \times 10^4 \text{ MPa}\cdot\sqrt{\text{m}}/\text{s}$ , compared to the quasi-static loading rates of 5 and  $0.4 \text{ MPa}\cdot\sqrt{\text{m}}/\text{s}$ , due to thermal blunting of the crack-tip

induced by adiabatic heating [11]. In rubber modified epoxy, R2, R6 and R10, although thermal blunting owing to localized adiabatic heating at the crack-tip may happen, its dependence at this high loading rate could be weak. Instead, the toughening mechanisms of rubber cavitation and matrix plastic deformation [2] are dominant and favored by the low loading rates, leading to the results displayed in Figure 7, especially when the rubber content is high. Again, further studies on the effects of loading rates on the relative amount of thermal blunting, cavitation and matrix plastic flow in these materials are essential to confirm the toughness results obtained.

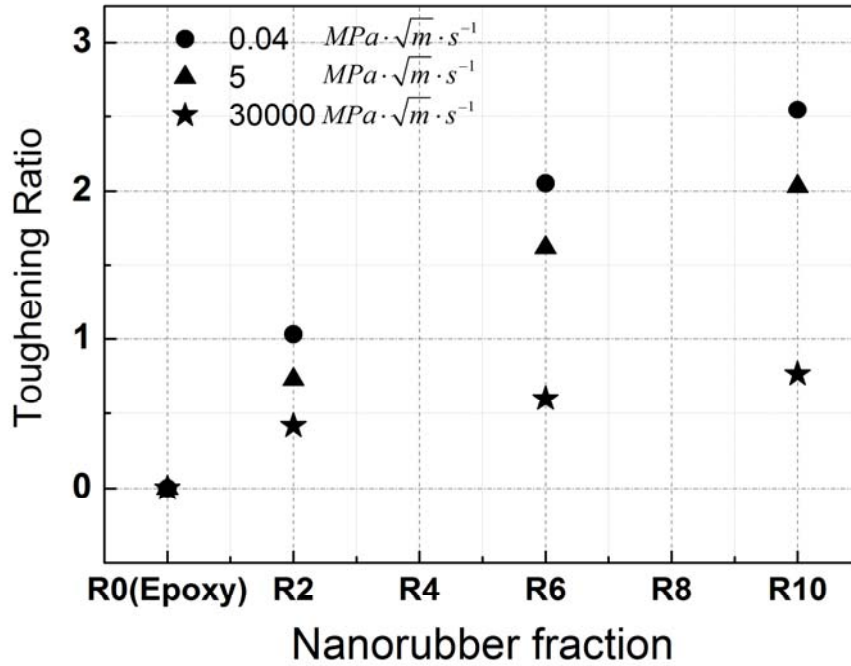


Figure 8 Normalized nano-rubber toughening efficiency of composites

A filler-toughening ratio parameter,  $\eta$ , can be used to evaluate the toughness increase associated with the nano-rubber particles. Thus,  $\eta$  is calculated from:

$$\eta = \frac{K_{IC} - K_{ICm}}{K_{ICm}} \quad (9)$$

where  $K_{IC}$ ,  $K_{ICm}$  are the toughness values of nano-rubber filled epoxies and neat epoxy matrix, respectively. Hence,  $\eta$  is a ratio of the net toughness caused by the nano-rubber presence over the net toughness of the epoxy matrix. Figure 8 plots the toughening efficiency parameter  $\eta$  of nano-rubber based on equation (9). In Figure 8, the toughening ratio of R2, R6 and R10 at each loading rate was best fitted, and their slopes could be found to have a distinct trend: it drops with increasing loading rates. As explained in the above section, this may be due to the reduced rubber cavitation and matrix plastic flow under the high strain rate.

## 5. Summary and Conclusions

The fracture performance of nano-rubber filled epoxies under a wide range of loading rates from

quasi-static ( $0.04 \text{ MPa}\cdot\sqrt{\text{m/s}}$ ) to Hopkinson bar ( $3 \times 10^4 \text{ MPa}\cdot\sqrt{\text{m/s}}$ ) tests were examined in terms of the fracture toughness and the toughening efficiency. Some important conclusions are summarized below:

- 1: The toughness of the nanocomposites increases with nano-rubber weight fraction.
- 2: The toughness of neat epoxy and 2 wt% rubber modified epoxy increases under dynamic loading due to thermal blunting.
- 3: The filler toughening efficiency drops with increasing loading rate. This is because increasing loading rates limit some toughening effects, such as cavitation and matrix plastic deformation, of rubber particles.

### Acknowledgements

Y-G Miao would like to thank the Chinese Scholarship Council for supporting him to work on this project at the University of Sydney, and the financial support by National Natural Science Foundation of China (No. 10932008) and the 111 project (No. B07050). H-Y Liu wishes to thank the Australian Research Council (ARC) for the support of this project through a Future Fellowship awarded to her (FT0992081, 2009-2013) tenable at the University of Sydney. Thanks are also due to Y Zeng and XS Du of the CAMT for sample preparation and helpful discussions during the various stages of this work. Use of the SHTB facility funded by the ARC LIEF (LE100100045) is much appreciated.

### References

- 1 H.-Y. Liu, G. T. Wang, Y.-W. Mai, Y. Zeng. *Composites: Part B*, 42( 2011) 2170–2175.
- 2 S. W. Koh, J. K. Kim, Y.-W. Mai. *Polymer*, 34(1993) 3446-3455.
- 3 S. Sahraoui, J. L. Lataillade, J. Pouyet, N. Skhiri. *Polymer testing*, 7(1987) 269-278.
- 4 V. M. F. Evora, A. Shukla. *Materials Science and Engineering: A*, 361(2003) 358-366.
- 5 ASTM D5045-99. Standard test methods for plane-strain fracture toughness and stain energy release rate of plastic materials; 1999.
- 6 Y. L. Li, K. T. Ramesh, E. S. C. Chin, *Materials Science and Engineering: A*, 371(2004) 359-370.
- 7 Y. L. Li, K. T. Ramesh, *International Journal of Impact Engineering*, 34(2007) 784-798.
- 8 Z. J. Xu, Y. L. Li, F. L. Huang, *Acta Mechanica Sinica*, 28(2012) 424-431.
- 9 J. Zhu, S. S. Hu, L. L. Wang, *International Journal of Impact Engineering*, 36(2009) 61-72.
- 10 W. F. Brown, Jr. And J. E. Srawley, *Plane strain crack toughness testing of high strength metallic materials*, ASTM STP 410, 1966, pp.12.
- 11 I. M. Low, Y.-W. Mai, *Journal of Materials Science*, 24(1989) 1634-1644.